



HAL
open science

Steam reforming and oxidative steam reforming for hydrogen production from bioethanol over Mg₂AlNiXHZOY nano-oxyhydride catalysts

Wenhao Fang, Yann Romani, Yaqian Wei, Mónica Jiménez-Ruiz, Hervé Jobic, Sébastien Paul, Louise Jalowiecki-Duhamel

► To cite this version:

Wenhao Fang, Yann Romani, Yaqian Wei, Mónica Jiménez-Ruiz, Hervé Jobic, et al.. Steam reforming and oxidative steam reforming for hydrogen production from bioethanol over Mg₂AlNiXHZOY nano-oxyhydride catalysts. *International Journal of Hydrogen Energy*, 2018, 43 (37), pp.17643-17655. 10.1016/j.ijhydene.2018.07.103 . hal-01887330

HAL Id: hal-01887330

<https://hal.science/hal-01887330>

Submitted on 24 Mar 2022

HAL is a multi-disciplinary open access archive for the deposit and dissemination of scientific research documents, whether they are published or not. The documents may come from teaching and research institutions in France or abroad, or from public or private research centers.

L'archive ouverte pluridisciplinaire **HAL**, est destinée au dépôt et à la diffusion de documents scientifiques de niveau recherche, publiés ou non, émanant des établissements d'enseignement et de recherche français ou étrangers, des laboratoires publics ou privés.



Distributed under a Creative Commons Attribution - NonCommercial 4.0 International License

Steam reforming and oxidative steam reforming for hydrogen production from bioethanol over $\text{Mg}_2\text{AlNi}_x\text{H}_z\text{O}_y$ nano-oxyhydride catalysts

Wenhao Fang^{a,b}, Yann Romani^a, Yaqian Wei^a, Monica Jimenez-Ruiz^c, Hervé Jobic^d, Sébastien Paul^a, Louise Jalowiecki-Duhamel^a

^aUniv. Lille, CNRS, Centrale Lille, ENSCL, Univ. Artois, UMR 8181 - UCCS - Unite de Catalyse et Chimie du Solide, 59000 Lille, France

^bSchool of Chemical Science and Technology, Key Laboratory of Medicinal Chemistry for Natural Resource - Ministry of Education, Functional Molecules Analysis and Biotransformation Key Laboratory of Universities in Yunnan Province, Yunnan University, 650091 Kunming, China

^cInstitut Laue-Langevin (ILL), 38042 Grenoble Cedex, France

^dInstitut de Recherches sur La Catalyse et l'Environnement de Lyon (IRCELyon), 69626 Villeurbanne Cedex, France

$\text{Mg}_2\text{AlNi}_x\text{H}_z\text{O}_y$ nano-oxyhydrides formation is evidenced during pre-treatment in H_2 at 450 °C of $\text{Mg}_2\text{AlNi}_x\text{O}_y$ nano-compounds leading to highly performant catalysts in ethanol conversion and H_2 formation, particularly at low temperature, through catalytic steam reforming (SRE) and oxidative steam reforming (OSRE). Total conversion of ethanol is obtained in SRE and OSRE with high stability. A higher production of H_2 ($60 \text{ L h}^{-1} \text{ g}_{\text{cat}}^{-1}$) can be achieved at a reaction temperature of 300 °C in OSRE conditions compared to SRE ($10 \text{ L h}^{-1} \text{ g}_{\text{cat}}^{-1}$) mainly because of a beneficial use of a high concentration of ethanol (14 mol %) in presence of O_2 . Moreover, carbon formation is decreased and a much lower input of energy of 50 °C is used to get a temperature of 300 °C when O_2 is added. Different physico-chemical characterizations and in particular in H_2 (TPR, H_2 -XRD, INS) and after tests allow to conclude that the presence of Ni^{2+} cations in strong interaction with other cations, anionic vacancies and hydride species on and inside the solid play an important role in the catalytic performance (conversion and selectivity) and stability.

Introduction

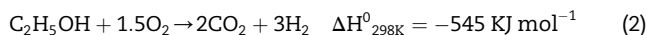
Hydrogen is globally viewed to be one of the most energy-efficient fuels on basis of high efficiency and cleanness [1,2]. Producing hydrogen from sustainable and environmentally benign process, instead of reforming petro-based sources, is of significant importance in bench and plant scales. Besides, the

wide-spread application of fuel cells becomes closer to reality, leading to refocus on hydrogen production technologies and process design [3–6] and on catalysts/electro-catalysts development. Catalytic transformation of bio-ethanol (ethanol usually selected as a simplified model), a fermentation product from biomass and a platform molecule in a bio-refinery, can be a neutral carbon-emission process since all carbon dioxide produced can be recycled back to plants, and

* Corresponding author.

E-mail address: louise.duhamel@univ-lille.fr (L. Jalowiecki-Duhamel).

because of its low toxicity and facile storage/transportation, ethanol lends itself very well to a distributed-production strategy. Hydrogen can be generated from ethanol through different technologies, as already reviewed [7–15]: steam reforming (SRE) (Eq. (1)), partial oxidation (POE) (Eq. (2)), and oxidative steam reforming (OSRE) processes, with the particular case of the so-called autothermal reforming (ATRE) process. SRE allows extracting more hydrogen atoms from ethanol and water molecules, nevertheless, such a strong endothermic reaction requires necessarily substantial energy input (≥ 650 °C). An alternative approach is POE, an exothermic reaction that exhibits fast start up and response time while potentially offering a more compact reactor design. In that case, the needed heating may be brought by simultaneous burning a portion of ethanol when oxygen or air is added to the feedstock. Though POE could be performed at relatively lower temperature, it is relatively less studied because of the high exothermicity of the reaction which could lead to hot-spots and usually related to deactivation of the catalyst.



The above-mentioned reactions have been studied over noble metals and transition metals with different bulk and supported catalysts, and compared on some catalysts [16–27]. The ethanol conversion and H_2 selectivity depended greatly on the catalysts, temperature, water/ethanol ratio, space velocity, contact time, and presence of O_2 . It has been reported that for some reactions nickel based catalysts comprising nanoparticles and strong metal-support interactions (SMSI) behave highly active and resistant to coking [7–15,28–37], and among which ex-hydrotalcite Ni–Mg–Al–O based compounds have been tested [38–45]. Thermal treatment of hydrotalcite (HT)-like compounds is a largely studied strategy for preparation of mixed oxides with high activity and mechanical strength, such as in H_2 production. The HT-like compounds enable to incorporate various metal cations such as Ni^{2+} , Co^{2+} and Cu^{2+} , and so they have been employed and studied as catalyst precursor or as catalyst support. As a matter of fact, it is known that the catalyst composition as well as preparation are of paramount importance whatever for catalyst activity, selectivity and stability.

The objective of this work is to compare hydrogen production through SRE and OSRE reactions at low temperature on the same highly active, selective, stable and inexpensive $\text{Mg}_2\text{AlNi}_x\text{H}_2\text{O}_y$ nano-oxyhydride catalysts. The influence of different parameters is analyzed, among them the pretreatment in H_2 of the catalyst and the ethanol concentration in the feed.

Experimental section

Catalysts preparation

Hydrotalcite-like compounds (noted HT) as catalyst precursor were synthesized by the co-precipitation method. An aqueous mixed solution of metal nitrates (1 mol L^{-1}) with an atomic

ratio of Mg:Al:Ni = 2:1:x (x = 1, 3 and 12) was drop-wise added into a mixed solution of NaOH/ Na_2CO_3 (1 mol L^{-1}) at room temperature till pH = 8. The slurry was vigorously stirred at 80 °C under condensation reflux for 18 h. The resulting solids were recovered by filtration and washed by excessive deionized water when the filtrate presented a neutral pH value. The solids were afterwards oven-dried at 120 °C for 15 h. The ex-hydrotalcites $\text{Mg}_2\text{AlNi}_x\text{O}_y$ nano-compounds were obtained by calcination of the precursors at 500 °C under an air flow for 4 h.

Catalytic reactions

SRE and OSRE reactions were conducted at atmospheric pressure with an up-flow quartz fixed-bed reactor (inner diameter 4 or 8 mm) containing the catalyst (0.008–0.05 g) fitted in a programmable oven, in the temperature range of 50–650 °C. When noted, the catalyst was previously in situ treated in H_2 for 10 h. For SRE, the N_2 gas stream (60 mL min^{-1}) was then fed to the reactor [44]. For OSRE, the O_2 – N_2 gas flow (60 mL min^{-1}) was used [45]. The water-ethanol mixture was pumped by HPLC pump into a heated chamber and vaporized. In order to analyze the influence of the concentration of ethanol, different liquid flows of the water-ethanol mixture were used while the $\text{H}_2\text{O}/\text{EtOH}$ molar ratio was always kept constant at 3/1. The liquid flows were 0.100, 0.010 and 0.005 mL min^{-1} corresponding to theoretical vapor flow of 80, 8 and 4 mL min^{-1} , respectively, leading to 14 mol% (concentrated conditions), 3 and 1 mol% of ethanol, respectively, checked by GC. The gases at the outlet of the reactor were taken out intermittently with the aid of a sampler directly connected to the system and analyzed on-line by gas chromatography (Thermo Fisher Scientific TRACE GC ULTRA) equipped with a thermal-conductivity detector (TCD) and a flame ionization detector (FID). The amount of solid carbon formed was determined by measuring the mass variation of the catalyst before and after test. The carbon formed is manually separated from the used catalysts and characterized as recovered.

Reaction data were collected as a function of time and reported after at least 5 h when a steady state was obtained, for each temperature. Catalytic performances were reported by ethanol conversion (X_{EtOH}) and products molar composition (C_i) (dry basis), based on the following equations (Eqs. (3) and (4)). In SRE, a H_2 yield (Y_{H_2}) of 6 mol of H_2 per mole of ethanol converted (Eq. (5)) is equivalent to 100% selectivity to H_2 in theory when all the hydrogen atoms from both ethanol and water are extracted (Eq. (1)). To report a H_2 yield in $\text{L h}^{-1} \text{g}_{\text{cat}}^{-1}$ and in $\text{g h}^{-1} \text{g}_{\text{cat}}^{-1}$ the H_2 concentration (in mol%) measured in effluent gas (by GC) and the starting (theoretical) gas flow rate are taken into account. However, it should be noted that there should be an increase of the flow rate with the production of a higher number of moles during the reaction according to the chemical equations (Eq. (1) or (2)).

$$X_{\text{EtOH}} = \frac{n_{\text{EtOH},\text{in}} - n_{\text{EtOH},\text{out}}}{n_{\text{EtOH},\text{in}}} \times 100\% \quad (3)$$

$$C_i = \frac{n_i}{\sum_{\text{products}} n_i} \times 100\% \quad (4)$$

$$Y_{H_2} = \frac{n_{H_2}}{n_{EtOH, in} X_{EtOH}} \quad (5)$$

Catalyst characterizations

The precise metal contents were analyzed by ICP-MS (CNRS Service Central d'Analyses) and the composition of solids was then deduced. For $Mg_2AlNi_xO_y$ nano-compounds, the Ni/ M_T ratio represents the nickel molar proportion in all the metals ($M_T = x + 3$, Ni/ $M_T = x/(x + 3)$).

The specific surface area was measured by N_2 physisorption at 77 K using BET method in a Micromeritics TriStar II 3020 Surface-Area and Porosimetry analyzer. The sample was previously out-gassed under vacuum at 150 °C for 3 h.

X-ray diffraction (XRD) was carried out with a Bruker D8 Advance X-ray diffractometer equipped with a fast detector type LynxEye with a copper anticathode. The patterns were registered in the 2θ domain (10–90°) with a measured step of 0.02°, and the time integration was fixed at 0.3 s. The average crystallites size was calculated by using the Scherrer equation.

In situ XRD in H_2 was performed in a Bruker D8 Advance type HT1200N X-ray diffractometer equipped with a fast detector type VANTEC with a copper anticathode. The sample was loaded into a quartz capillary cell that was attached to a flow system (3% H_2 - 97% Ar in vol., 10 °C min^{-1}).

X-ray photoelectron spectroscopy (XPS) analysis was performed in a Thermo VG Escalab 220 XL spectrometer under ultrahigh vacuum, using a twin Al X-ray source (1486.6 eV) at a pass energy of 40 eV. The solids in the form of pellets were fixed on a copper holder with copper tape. The charge effect was adjusted by reference to the C 1s peak at 284.8 eV for all the samples before the reaction.

H_2 -TPR was performed in a Micromeritics Autochem II Chemisorption analyzer, and the H_2 consumption was measured by a TCD detector. The sample was treated in the 5% H_2 - 95% Ar (in vol.) mixture with a flow rate of 30 mL min^{-1} . The temperature was increased to 1000 °C at a heating rate of 10 °C min^{-1} .

Inelastic neutron scattering (INS) experiments were carried out in the Lagrange spectrometer at the Institut Laue Langevin, Grenoble France. 36 g of the solid was placed in a stainless steel container and treated at 450 °C in high purity H_2 (10 h)

and sealed. INS was analyzed at 10 K by using a Cu monochromator. The scattering cross-section is much greater for hydrogen (80 b) than for other elements (5 b); therefore, INS emphasizes the motions of hydrogen species.

O_2 -TPO was performed in a Micromeritics Autochem 2920 analyzer. The sample was treated in the 5 vol% O_2 –95 vol% He mixtures with a flow rate of 50 mL min^{-1} . The temperature was increased to 1000 °C at a heating rate of 5 °C min^{-1} . The desorption species from the sample were detected by using a OmniStar GSD 300 O mass spectrometer.

Raman spectra of carbonaceous species were acquired on a Labram Infinity HORIBA JOBIN YVON Raman spectrometer using a visible laser with a wavelength of $\lambda = 532$ nm at room temperature.

TEM images were obtained by a FEI Tecnai G2 20 transmission electron microscope at an acceleration voltage of 200 kV. The sample was previously ultrasonically dispersed in acetone, and then drops of the suspension were applied onto a copper grid-supported transparent carbon film.

Results and discussion

Steam reforming of ethanol (SRE)

To investigate the influence of pre-treatment temperature (T_T) on the $Mg_2AlNi_{12}O_y$ catalyst, different pre-treatment temperatures were selected. Fig. 1 compares SRE performances in harsh conditions (as a high EtOH concentration of 14 mol% is used) on the non-treated and pretreated in H_2 $Mg_2AlNi_{12}O_y$ catalyst as a function of reaction temperature. The $Mg_2AlNi_{12}O_y$ catalyst without pre-treatment is unable to convert any ethanol at low temperature (≤ 250 °C). Conversion starts to be detectable from 300 °C and is lower than 10% up to 400 °C; even it can approach to 20% at 450 °C. Hydrogen and acetaldehyde are the only products obtained during the whole temperature range investigated, however, H_2 starts to be really observed at 350 °C. Clearly the catalyst starts to be activated under the reaction mixture at about 300 °C. After pre-treatment in H_2 at 450 °C, the obtained catalyst demonstrates quite different behavior. A very good catalytic performance in low temperature range (≤ 300 °C) is obtained with an

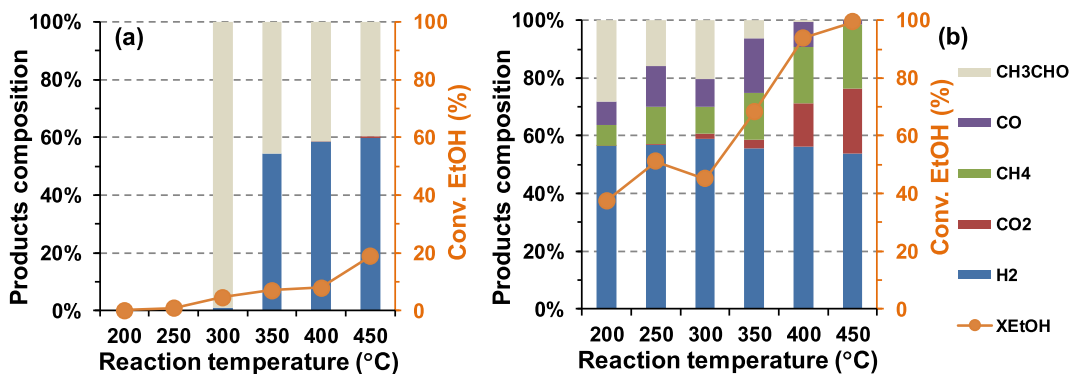


Fig. 1 – Comparison of SRE (14 mol% EtOH) over the $Mg_2AlNi_{12}O_y$ catalyst (0.05 g) with (a) no pre-treatment and (b) pre-treatment in H_2 450 °C.

optimum of ethanol conversion (51%) at 250 °C even if conversion globally increases with temperature. The observed main products are H₂, acetaldehyde, methane and CO. CO₂ formation largely emerges from 400 °C meanwhile acetaldehyde disappears. The SRE was studied at low temperatures (200 and 250 °C) in order to better see the variations with respect to ethanol conversion and products distribution. As shown in Fig. 2, no ethanol is converted into any products at low temperature, when the Mg₂AlNi₁₂O_γ catalyst is pre-treated in H₂ at 163 °C. For reaction temperature of 250 °C, ethanol conversion rapidly increases to 37% with T_T at 365 °C, and keeps rising to 51% with T_T at 450 °C. Ethanol conversion follows relatively similar evolution for reaction temperature at 200 °C, with 35% of conversion with T_T at 450 °C. The products distribution exhibits very similar evolution relatively independent of the pre-treatment temperature (350–450 °C). H₂ formation maintains about 57% (in mol., dry basis) and CO₂ formation constantly stays zero whatever the reaction temperature. It makes sense that the strong endothermic SRE reaction hardly takes place at these low temperatures. CO and CH₄ formation clearly present higher values at 250 °C compared to 200 °C, while it is inverse for acetaldehyde formation. This is in agreement with the discussion on the thermodynamics influence of reaction temperature [46]. With the temperatures investigated, dehydrogenation (Eq. (6)) and/or decomposition of ethanol (Eqs. (7) and (8)) appear as the main reactions. The decomposition reaction is accentuated at 250 °C when the Mg₂AlNi₁₂O_γ catalyst is activated in H₂ at 450 °C. It has been shown for this series of catalysts that increasing Ni content and pre-treatment temperature promote the formation of carbon [43]. Pre-treating the Mg₂AlNi₃O_γ catalyst at higher temperature than 450 °C leads mainly to significantly higher carbon formation instead of activity, even if slightly higher EtOH conversion might be obtained.



Fig. S1 shows the influence of Ni content of Mg₂AlNi_xO_γ catalysts pretreated in H₂ at 450 °C on the catalytic

performances in harsh conditions. Ethanol conversion, as well as products distribution, are strongly associated with Ni content. With the increase of Ni content, ethanol conversion undergoes a global rise, showing that higher Ni content facilitates SRE process (Eq. (1)) in agreement with the well-known Ni activity. Total conversion of ethanol with formation of around 55% of H₂ and about 22% of CO₂ are observed at Ni/M_T = 0.8. When increasing Ni content H₂ formation decreases from about 70% to 55% and CH₃CHO formation rapidly declines and reaches zero when Ni/M_T = 0.8, whereas in the meantime CH₄ and CO₂ formations increase, while CO formation exhibits an optimum at Ni/M_T = 0.5. Numerous different reactions can take place, and have been largely reviewed [7–15], acetaldehyde can be obtained by ethanol dehydrogenation (Eq. (6)) and decomposition of ethanol (Eq. (7)) and/or acetaldehyde (Eq. (8)) lead to the formation of methane and CO that can be followed by further transformation. In complement to SRE reaction, the results demonstrate that higher Ni content promotes the decomposition of ethanol and/or acetaldehyde as methane increases, however as CO presents an optimum it seems to be further transformed. It is probably due to carbon formation by disproportionation of CO (Eq. (9)), in agreement with the higher quantity of carbon formation observed on the Mg₂AlNi₁₂O_γ catalyst. As a matter of fact carbon formation increases with Ni content [44]. For low Ni content, CO could be transformed by water gas shift reaction (Eq. (10)).



To better see the real catalytic behavior of the Mg₂AlNi₁₂O_γ catalyst, this catalyst was tested with a very low mass of 8 mg (Fig. 3). Total conversion can be reported in the initial stage (1 h). Afterwards the activity decreases with time on stream and stabilizes after 5 h (40%). A decrease of ethanol conversion is observed with in such a case appearance of acetaldehyde. The obtained values are high compared to literature when taking into account the reaction conditions, the absence of noble metal and the low mass of catalyst involved [15,47,48]. The Ni₅₀MgAl catalyst exhibited activity lower than 30% when the reaction temperature is below 450 °C working with 9.2 mol

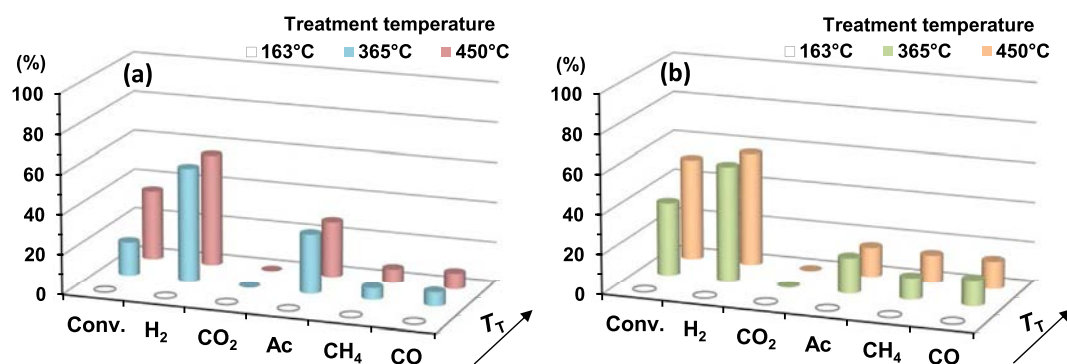


Fig. 2 – Influence of pre-treatment temperature in H₂ on SRE (14 mol% EtOH) at (a) 200 °C and (b) 250 °C on the Mg₂AlNi₁₂O_γ (0.05 g) catalyst.

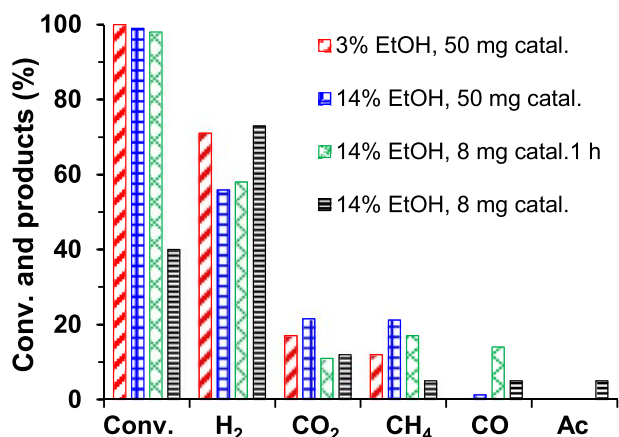


Fig. 3 – Conversion of ethanol in SRE and gas phase products distribution at 450 °C on the $Mg_2AlNi_{12}O_Y$ catalyst. Ac: acetaldehyde.

% of ethanol [38]. It is important to recall that the high conversion of ethanol that is injected in high concentration leads to a high production of gases, while H_2 formation relative to all the gas phase products (dry basis) maintains about 55% (in mol.). Moreover, to avoid any problem caused by volume variation when a high concentration of gases was produced, the efficiency of the $Mg_2AlNi_{12}O_Y$ catalyst was thoroughly studied by its capacity to produce hydrogen from SRE in diluted conditions (EtOH at 3%) while $H_2O/EtOH$ molar ratio was kept constant at 3 (Fig. 3 and Fig. S2). At 450 °C, the catalyst (0.05 g) is able to completely convert ethanol to H_2 , CO_2 and CH_4 (no CO formed), with a H_2 yield of $3 \text{ mol mol}_{EtOH}^{-1}$ (Fig. S2). On the present catalyst, the activity is very high at 450 °C and almost no variation is observed on the conversion with only a slight decrease when ethanol concentration is increased from 3 to 14%. Meanwhile, the products distribution is influenced by the decrease of ethanol concentration, with an increase in H_2 proportion (among the gas phase products) and a decrease of the others products (CO being already almost not formed). At 650 °C the $Mg_2AlNi_{12}O_Y$ catalyst allows obtaining a H_2 production of $4.8 \text{ mol mol}_{EtOH}^{-1}$ (Fig. S2a). It is important to mention that working at high temperature water gas shift (WGS) equilibrium (Eq. (10)) does not allow reaching the theoretical value of $6 \text{ mol mol}_{EtOH}^{-1}$ (on basis of Eq. (1)). The obtained value at 650 °C is comparable to some values reported on Ni-based catalysts, taking into account the reaction conditions; with H_2 yields of $5.0 \text{ mol mol}_{EtOH}^{-1}$ on $Ni_{50}ZnAl$ catalyst ($H_2O/EtOH = 6$) and $5.1 \text{ mol mol}_{EtOH}^{-1}$ on Ni/Mg_2AlO_Y catalyst ($H_2O/EtOH = 8.4$) [38,39]. As a matter of fact, H_2 yield can be promoted by increasing water content compared to the stoichiometry of SRE process ($H_2O/EtOH = 3$). Moreover, the present result seems also competitive compared to other inexpensive catalysts, such as Cu- and Co-based mixed oxides [49,50]. Besides, complete ethanol conversion is achieved at temperatures as low as 250 and 300 °C using lower EtOH concentration (1%) (Fig. S2b) and only H_2 , CO_2 and CH_4 are formed in gas-phase. No CO or acetaldehyde is obtained. Methane transformation is logically more pronounced at 300 °C (compared to 250 °C); as a result, a higher proportion of

H_2 is obtained. The H_2 yield is close to $3 \text{ mol mol}_{EtOH}^{-1}$ at 300 °C, which can correspond to 100% of H_2 yield in total decomposition of ethanol to hydrogen. The stability of the catalyst was analyzed more deeply on the $Mg_2AlNi_{12}O_Y$ compound. As reported in Fig. 4a, the catalyst shows a good stability after 125 h of reaction at 300 °C without any sign of deactivation even if carbon is formed. It has been reported that Rh–Co/CeO₂ catalyst can lead to a CO-free H_2 yield of $4.3 \text{ mol mol}_{EtOH}^{-1}$ at 300 °C, however, the value was obtained using a high $H_2O/EtOH$ ratio at 10 [51]. Besides, the value corresponded to an initial state obtained after only 25 min. In another study, Rh–Fe/Ca–Al₂O₃ catalyst was developed as efficient and stable catalyst for ESR at low temperature. A H_2 yield of $3.5 \text{ mol mol}_{EtOH}^{-1}$ was reported at 300 °C using a large amount of water ($EtOH/H_2O/N_2 = 1/10/89$) [52]. Moreover, CO was formed in the gas-phase products at 300 °C but could be suppressed at 350 °C. Furthermore, it was also reported that total ethanol conversion and stable products distribution can be obtained accompanied with carbonaceous deposits on a noble metal-based catalyst (CeZrCoRh) [53].

Oxidative steam reforming of ethanol (OSRE)

The $Mg_2AlNi_3O_Y$ catalyst (0.03 g) pre-treated in H_2 at 450 °C was studied for H_2 production in OSRE of ethanol ($EtOH/H_2O/O_2/N_2 = 1/3/1.6/1.3$, with EtOH at 14%). On this compound, the reaction must be started at least at 180 °C, and then the oven temperature is decreased to 50 °C. The catalyst completely converts ethanol and O_2 with a H_2 formation of about 45% (in mol., dry basis) at a stable measured reaction temperature of about 260 °C (Fig. 4b). The other gas phase products formed are mainly CO_2 (41%) and CO (13%). The catalytic activity is fairly stable after 75 h on stream without any sign of deactivation even if some solid carbon is formed.

Furthermore, depending on the Ni content of the $Mg_2AlNi_xO_Y$ catalysts pre-treated in H_2 at 450 °C, complete conversions of ethanol and oxygen are obtained with a good stability after at least 20 h on stream but not at the same measured reaction temperature (Fig. S3). On the lowest Ni content catalyst, the catalytic reaction can only be started at about 390 °C, then the oven temperature can be decreased and the required minimal oven temperature to maintain the reaction is at 215 °C while the measured reaction temperature is at 405 °C. It can be noticed that for this compound, no carbon formation is observed. For the other catalysts ($x > 1$) the initial oven temperature is of about 200 °C and depending on the catalyst can be as low as 155 °C while it slightly increases when Ni content decreases. When the Ni content is high enough ($x > 1$), the oven temperature can be reduced down to 50 °C and the measured temperature maintains depending on the catalyst, at least at 260 °C. The main products obtained in the gas-phase are H_2 , CO_2 and CO (Fig. S3). Increasing Ni content leads to an increase of H_2 formation up to about 45%, then it slightly decreases when $x > 3$. The formation of CO_2 increases from 37 to 46% for the highest Ni content, while CO formation decreases from 28 to 12%. Acetaldehyde and methane are lower than 1% whatever the Ni content. Solid carbon increases when $x \geq 3$ [45]. The $Mg_2AlNi_1O_Y$ catalyst leads to different products composition, with a higher

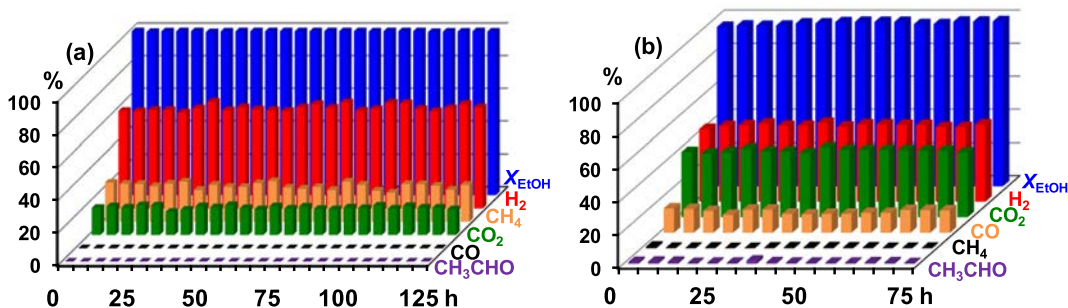


Fig. 4 – Time course of a) $Mg_2AlNi_{12}O_y$ catalyst (0.05 g) for SRE (1 mol% EtOH) at 300 °C and b) $Mg_2AlNi_3O_y$ catalyst (0.03 g) pre-treated in H_2 at 450 °C for OSRE (14 mol% EtOH) with an oven temperature at 50 °C (reaction mixture is $EtOH/H_2O/O_2/N_2 = 1/3/1.6/1.3$ and measured reaction temperature is of 260 °C).

formation of CO that can be explained by the absence of carbon formation.

Only few studies reported OSRE at such a low temperature [27–29]. Sato et al. reported in OSRE at very low temperature (100 °C) a H_2 yield close to 100% on $Ni/Ce_{0.5}Zr_{0.5}O_2$ and Ni/CeO_2 catalysts using a feed gas mixture containing $EtOH/H_2O/O_2/(N_2+Ar) = 1/8/1/4$ [54]. The conversions and H_2 formation rates were measured after 30 min in repeated cycles. For the low temperature range OSRE (300–450 °C), some best performing catalysts have been reported [9]. $Ni-Co/ZnO-Al_2O_3$ catalyst was shown to perform at 300 °C allowing total conversion of ethanol with a H_2 selectivity at about 50% when feeding a mixture of $EtOH/H_2O/O_2/N_2 = 1/3/0.4/1.2$, however, with a high formation also of acetaldehyde [55]. $Pt-Ni/CeO_2-SiO_2$ catalysts exhibited total ethanol conversion between 350 and 600 °C and hydrogen yields very close to thermodynamic values at $T > 450$ °C under a reaction mixture of 10% $C_2H_5OH:5\% O_2:40\% H_2O:45\% N_2$ with a WHSV of $4.1 h^{-1}$ [56]. The $CoZn_{2.4}Al_{1.9}$ ex-hydrotalcite mixed oxide ($EtOH/H_2O/O_2/N_2 = 1/2.28/0.36/N_2$, total flow of $120 mL min^{-1}$) and the $La_{0.9}Ce_{0.1}NiO_3$ perovskite-type oxide ($EtOH/H_2O/O_2/N_2 = 2.5/7.5/1.25/88.75$) allowed obtaining total conversion of ethanol with a H_2 formation close to 60 mol% at 575 °C and at 500 °C, respectively [57,58]. Therefore, the present catalysts show high performance for OSRE reaction while using high concentration of ethanol (14%).

Comparison between SRE and OSRE at low temperature

The developed catalysts turn out highly active and stable toward H_2 production from catalytic reforming of ethanol. It is usually reported that OSRE presents some significant benefits. The exothermic contribution of oxidation reactions may reduce the external heat supply and air co-feeding tends to decrease carbon deposits on catalysts [59]. In the present study an $O_2/EtOH$ ratio close to the one required for partial oxidation (Eq. (2)) has been used, and a particularly low temperature has been studied. As carbon formation increases with Ni content, the high Ni content $Mg_2AlNi_{12}O_y$ catalyst is taken for this deep analysis. On the pretreated in H_2 at 450 °C $Mg_2AlNi_{12}O_y$ catalyst (Table 1), total conversion of ethanol is obtained at 300 °C working with a low concentration of EtOH (1%) in SRE conditions and in high concentration of EtOH (14%) in OSRE conditions (Fig. 5a). In high concentration of EtOH (14%), much lower conversion is obtained at 300 °C in SRE conditions (Fig. 5b). Moreover, it has to be noted that a higher catalyst mass is used for SRE conditions and to be recalled that much lower energy (extra heating at only 50 °C) is required here for OSRE. Clearly, the conversion of ethanol is increased significantly by the addition of O_2 into the reactant mixture, as often accepted in the literature, even if there are some exceptions [9,16,17,20,24]. Moreover, for the same EtOH concentration, lower carbon formation is obtained in OSRE, in

Table 1 Comparison of H_2 production from SRE and OSRE at 300 C on the $Mg_2AlNi_xO_y$ catalysts pre-treated in H_2 at 450 C.

Feed composition	Catalyst mass (g)	Time (h)	EtOH Conv. (%)	H_2 among products (mol%)	H_2 in effluent (mol%)	H_2 production ($L h^{-1} g_{cat}^{-1}$)	H_2 production ($g h^{-1} g_{cat}^{-1}$)	Carbon formation ($g h^{-1} g_{cat}^{-1}$)
$EtOH/H_2O/N_2 = 1/3/96$ (mol%) ^a	0.05	125	100	60 ^b	1.1	0.8	0.07	0.02
$EtOH/H_2O/N_2 = 14/42/44$ (mol%) ^a	0.05	5	45	59	6.4	10.7	0.96	0.28
$EtOH/H_2O/O_2/N_2 = 1/3/1.6/1.3$ (EtOH: 14 mol%) ^{c,d,e}	0.03	75	100	44	18.2	51.1	4.56	0.03
$EtOH/H_2O/O_2/N_2 = 1/3/1.6/1.3$ (EtOH: 14 mol%) ^{a,e}	0.03	20	100	42	21.4	60.0	5.36	0.14

^a Obtained on the $Mg_2AlNi_{12}O_y$ catalyst.

^b 3.0 mol mol $_{EtOH}^{-1}$ is reported in text.

^c Obtained on the $Mg_2AlNi_3O_y$ catalyst.

^d Measured reaction temperature at 260 °C.

^e Oven temperature fixed at 50 °C.

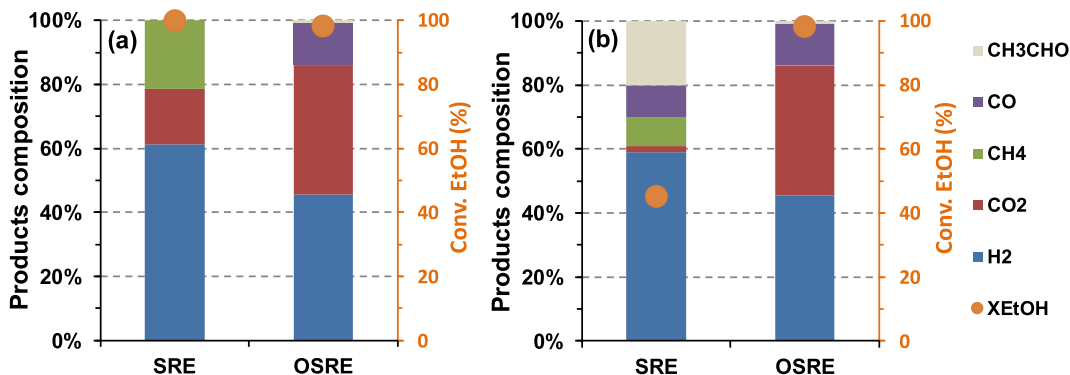
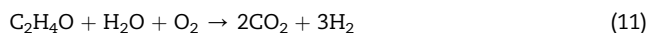


Fig. 5 – Comparison at 300 °C on the pre-treated in H₂ at 450 °C Mg₂AlNi₁₂O_γ catalyst of (a) SRE (1 mol% EtOH) and OSRE (14 mol% EtOH) reactions. SRE: 0.05 g catalyst, data is an average value obtained during 125 h of reaction; OSRE: 0.03 g catalyst, data is an average value obtained during 20 h of reaction, and (b) SRE (14 mol% EtOH) and OSRE (14 mol% EtOH) reactions. SRE: 0.05 g catalyst, data is an average value obtained during 5 h of reaction; OSRE: 0.03 g catalyst, data is an average value obtained during 20 h of reaction.

agreement also with literature. More interestingly, much higher production of H₂ is obtained in OSRE conditions mainly due to the high concentration of EtOH used, and the low mass of catalyst that could be involved. Furthermore, the obtained values for H₂ production in OSRE (about 50 and 60 L h⁻¹ g_{cat}⁻¹) are quite high and of the same order compared to the H₂ production of 44 L h⁻¹ g_{cat}⁻¹ previously reported on Ni/Ce_{0.5}Zr_{0.5}O_{2-x} compounds at low temperature [54].

Quite different products distribution in gas phase is observed between SRE and OSRE at a low temperature of 300 °C. When considering the conditions in which total conversion of ethanol is obtained (Fig. 5a), on one hand, H₂ formation is about three times more than that of CO₂ in SRE (as expected from Eq. (1)) whereas they are almost equal in OSRE (not so far compared to what is expected from Eq. (2)). On the other hand, methane is the only by-product for SRE while CO is the only by-product (with very small quantities of methane and acetaldehyde) for OSRE. If hydrogen production is the goal, low CH₄ is desirable because it contains hydrogen. When high concentration of EtOH (14%) is used (Fig. 5b), for SRE different products distribution is obtained, with formation of mainly H₂ and acetaldehyde, with lower quantities of CH₄ and CO and very small quantity of CO₂.

Apart from the above-discussed numerous possible reactions, burning a portion of ethanol through OSRE result in higher CO₂ formation. When acetaldehyde is formed, the very high reactivity of aldehyde allows it very easily to further undergo OSRE to produce H₂ and CO₂ (Eq. (11)), that probably explains the results obtained here [9]. WGS reaction that is slightly exothermic is favored at low temperature and enables the transformation of CO (Eq. (10)). Besides, in the presence of O₂, the partial oxidation of methane (Eq. (12), which is also exothermic) could lead to the formation of H₂ and CO (or CO₂ at higher O₂ concentration).



The catalysts show good catalytic stabilities in terms of activity and gas phase products distribution for SRE and OSRE, even when solid carbon is also formed among the products and observed after reaction. Graphitic filamentous carbon is formed, as shown in Fig. 6 by different techniques (TPO, Raman, TEM). One can remark that depending on the catalyst and conditions applied different degrees of graphitization of the carbon formed are observed by Raman, however globally the same type of carbon is obtained. The stability of the activity is supposed to be related to this type of carbon.

Usually lower O₂/EtOH ratios and higher temperatures have been analyzed in literature. On Ni/CeO₂-ZrO₂ catalyst, Biswas et al. analyzed the influence of the O₂/EtOH ratio up to 1.5 in the presence of a high concentration of water (H₂O/EtOH = 8) and have shown that in presence of O₂, the catalytic activity was significantly higher and the effect was more pronounced at lower temperature (<450 °C) [18]. The catalyst activity was enhanced significantly, and at temperatures less than 500 °C, the hydrogen yields were higher than without oxygen. Moreover, they observed that coke formation was reduced significantly in the presence of small amount of oxygen. Wang et al. compared the catalytic performance for SRE and OSRE on La_{0.7}Ca_{0.3}Fe_{0.7}Co_{0.3}O₃ catalyst at temperatures higher than 550 °C to get 100% ethanol conversion [21]. Hydrogen selectivity decreased as reaction became to OSRE from SRE. The lower selectivity for hydrogen in OSRE was ascribed to two reasons, one was the lower carbon deposition under OSRE condition and the other one was that more CO₂ was generated under OSRE by oxidation with O₂ which can promote reverse water gas shift reaction consuming H₂. The performance of Co/CeO₂ and K-Co/CeO₂ catalysts in both SRE (H₂O/EtOH = 9/1) and OSRE (H₂O/EtOH/O₂ = 9/1/0.7) processes were analyzed by Greluk et al. [26], the optimum temperature of both processes was 540 °C. The small oxygen addition allowed to decrease the coke formation on the catalyst surface and to reduce slightly its deactivation. But higher hydrogen production was obtained in absence of oxygen. On a modified PtRu/ZrO₂ catalyst Chiou et al. have shown that the OSRE reaction requires a higher temperature (390 °C) to achieve 100%

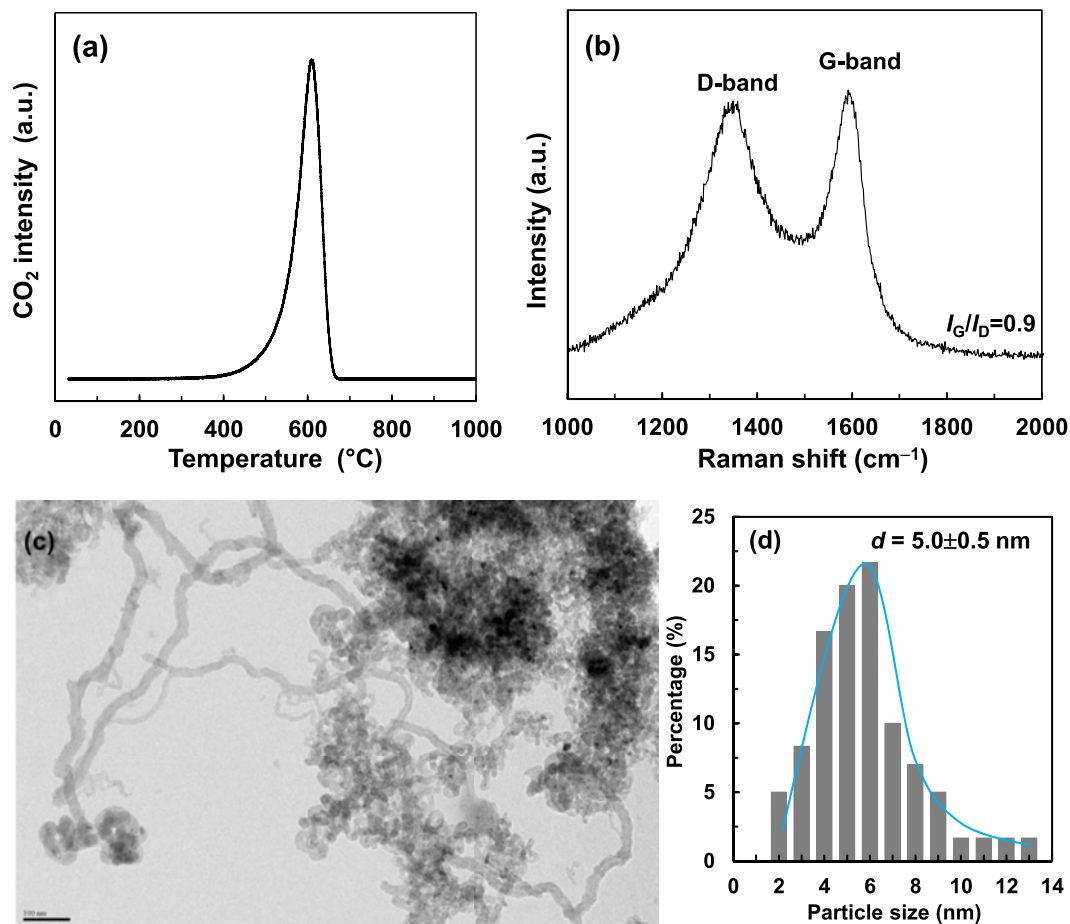


Fig. 6 – Characterizations of the $Mg_2AlNi_{12}O_y$ catalyst and solid carbon formed after SRE at 300 °C with 1 mol% EtOH for 125 h. Solid carbon: (a) O_2 -TPO profile, and (b) Raman spectrum. Catalyst and carbon: (c) TEM image and (d) corresponding distribution of particles size of Ni species.

ethanol conversion than the SRE reaction [20]. The $H_2O/EtOH$ molar ratio was 13 for the SRE reaction, while the $O_2/EtOH$ molar ratio was 0.26, and the $H_2O/EtOH$ molar ratio was 4.86 for the OSRE reaction. In their case a more pronounced coke formation was observed in the OSRE reaction [20]. Palma et al. studied Pt–Ni/CeO₂/SiO₂ catalysts in the 300–600 °C temperature range applying a $H_2O/EtOH$ molar ratio of 4 and an $O_2/EtOH$ molar ratio of 0.5 in OSRE conditions [24,25]. For $T < 430$ °C, when adding O_2 , ethanol conversion was higher in comparison with the values obtained in SRE reaction. In particular, at $T = 300$ °C, the conversion recorded at $30000\ h^{-1}$ for OSRE was similar to the value obtained at the same temperature and lower space velocity ($20000\ h^{-1}$) without O_2 . Moreover, the results of stability tests revealed that O_2 addition in the reforming mixture improved catalyst stability, which was maintained for 70 h. Oxygen co-feeding strongly improved catalyst durability, resulting in a carbon formation rate reduction. Furthermore, Velu et al. compared SRE and OSRE at 300 °C on CuNiZnAl mixed oxide catalysts [16], using a lower concentration of O_2 in OSRE conditions ($O_2/EtOH = 0.4$). They have shown differences between the experimental products distribution and the expected equilibrium compositions (calculations assuming 100% EtOH conv.) and reported

that the partial oxidation of EtOH along with SRE under their experimental conditions drives to non-equilibrium distribution of products in line with a previous literature report [60].

Ex situ characterizations of $Mg_2AlNi_xO_y$ catalysts by ICP-MS, N_2 physisorption, XRD and XPS

The co-precipitation method allows synthesis of well-dispersed multi-component metal-oxide materials starting from hydrotalcites compounds (Fig. S4, Table 2). The $Mg_2AlNi_xO_y$ nano-compounds display large specific surface areas between 120 and $200\ m^2\ g^{-1}$, which depend on the different Ni contents. The surface area of the oxides is increased compared to the HT precursors. The average crystallites size of the oxides calculated from XRD is small and distributed in the 3–6 nm range. XRD shows the presence of hydrotalcite phase for the precursor and crystalline phases of Mg-(Al)–Ni–O solid solution, and/or NiO and/or MgO for the oxides, because XRD diffraction patterns of these phases are overlapping each other. After test the oxide phases well remain, however an increase of the average crystallites size is observed after OSRE. Metallic nickel (Ni^0) with a similar average crystallites size is observed after treatment in H_2 at

Table 2 – Ni content, specific surface area and average crystallites size of the compounds.

Compound	Ni content (wt%) ^a	Ni/M _T molar ratio ^a	S _{BET} (m ² g ⁻¹)	d ₁ (nm)	d ₂ (nm)	d ₃ (nm)
Mg ₂ AlNi ₁ O _Y HT	15	0.24	76	–	–	–
Mg ₂ AlNi ₃ O _Y HT	31	0.54	46	–	–	–
Mg ₂ AlNi ₁₂ O _Y HT	42	0.81	137	–	–	–
Mg ₂ AlNi ₁ O _Y	22	0.24	127	3.6 ^b	3.6 ^c	–
Mg ₂ AlNi ₃ O _Y	44	0.50	168	3.9 ^b	4.0 ^c	–
Mg ₂ AlNi ₁₂ O _Y	62	0.80	196	5.9 ^b	5.5 ^c	5.0 ^d
Mg ₂ AlNi ₁₂ O _Y after SRE at 300 °C with 1 mol% EtOH	–	–	–	–	5.4 ^e	5.0 ^f
Mg ₂ AlNi ₃ O _Y after OSRE at 260 °C with 14 mol% EtOH	–	–	–	–	17 ^e	22 ^f

^a Measured and deduced by ICP-AES technique, Ni/M_T molar ratio = x/(x + 3). Average crystallites size of ^b oxide deduced from XRD using the Scherrer equation, ^c oxide and ^d metallic nickel deduced from in situ XRD in H₂ at 450 °C for 10 h, ^e oxide and ^f metallic nickel deduced from XRD after test under the given conditions.

450 °C for the compound with the highest Ni content. However, after test metallic nickel (Ni⁰) is observed for the two Mg₂AlNi_xO_Y catalysts (with x = 3 and 12) with an average crystallites size which increases also mainly after OSRE.

XPS reveals the presence of Ni²⁺ cations (Table S1) with a BE of the Ni 2p_{3/2} peak at about 855.6 eV for the Mg₂AlNi_xO_Y catalysts when x > 1 and even slightly higher at 856.1 eV when x = 1. These values are higher than the BE reported for bulk NiO (853.7–854.6 eV), but very close to the one observed for NiAl₂O₄ (856.0 eV) and very similar to the previously reported value for Ni–Mg–Al mixed oxides (855.5 eV) [41]. These results demonstrate the strong interactions between Ni²⁺ species with Al³⁺ species and Mg²⁺ species. For the oxides, the O 1s core level presents two major oxygen species at 530.6 eV, typical O²⁻ lattice species, and at 531.7 eV, that can be related to oxygen species in hydroxyl groups (OH⁻) [61] also present on the HT precursors. After test the cations in strong interaction are still present, as shown by the BE values of the Ni 2p_{3/2} peak positions maintaining the values observed on the oxides and even reaching the values obtained on the HT starting materials. Besides, the FWHM increase evidences the presence of different Ni species. The BE for oxygen species corresponds mainly to the presence of hydroxyl groups as observed also on the HT starting compounds. The Ni/M_T molar ratio on surface appears relatively lower than that in bulk (ICP-MS) in the Mg₂AlNi_xO_Y compounds, probably due to some segregation on the calcined solids. A relatively linear function of Ni/M_T on surface versus Ni/M_T in bulk is obtained (result not shown), showing a good respect to the homogeneous distribution of nickel species inside Mg₂AlNi_xO_Y solids.

All the above results reveal that Mg₂AlNi_xO_Y catalysts present O²⁻ species and hydroxyl groups at the surface and exhibit strong interactions between Ni²⁺ species and other cations that are well maintained even after test and with a high Ni content, in agreement with the presence of a solid solution.

In situ in H₂ characterizations of Mg₂AlNi_xO_Y catalysts (TPR, XRD and INS)

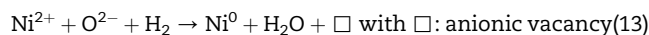
Mg₂AlNi_xO_Y nano-compounds show a main broad TPR peak between 550 and 755 °C that shifts to lower temperature when Ni content increases (Table 3). For low Ni content the strong interactions between nickel species and Al³⁺ and/or Mg²⁺

Table 3 – Data obtained from TPR.

Catalyst	Main peak (°C)	H ₂ cons. ^a (mL g ⁻¹)	H/Ni
Mg ₂ AlNi ₁ O _Y	755	105	2.5
Mg ₂ AlNi ₃ O _Y	620	202	2.4
Mg ₂ AlNi ₁₂ O _Y	560	279	2.4

^a After integration of all hydrogen consumed during TPR.

cations make the solid more difficult to reduce while the reducibility of the compound becomes closer to that of bulk NiO when Ni content increases. However, as the temperature is still higher compared to the one needed to reduce bulk NiO (370 °C), strong interactions among cations still exist in Mg₂AlNi_xO_Y compound even for high Ni content. Therefore, for a treatment temperature in H₂ at 450 °C only a partially reduced solid is obtained, as 450 °C corresponds to a temperature before the TPR peak. However, as the TPR peak presents a shift, the compounds are not reduced to the same extent. The obtained H/Ni ratios at about 2.4 (Table 3) show that a higher quantity of hydrogen is consumed by the solids compared to what is required (Eq. (13)), that is probably due to a hydrogen “spillover” phenomenon.



In situ XRD in H₂ at 450 °C (10 h) reveals that the oxide phases are well present in all the studied compounds (Fig. 7) even if some small Ni⁰ nanoparticles are observed with the highest Ni content (Table 2). The peaks of oxides become less intense on Mg₂AlNi₃O_Y and Mg₂AlNi₁₂O_Y compounds. This treatment conditions allows obtaining partially reduced solids with the simultaneous generation of anionic vacancies, in agreement with TPR results. The average crystallites size shows almost no variation with the treatment in H₂ (Table 2). Moreover, compared to the starting oxide material, a shift to lower 2θ values is observed in agreement with the insertion of hydrogen species of hydridic nature in the compound. As a matter of fact, the ionic radius of hydride ion is higher than the one of an O²⁻ species leading to an expansion of the lattice, as already observed on CeNi_xO_Y mixed oxides that were shown to form oxyhydrides [62].

The treatment of solids with H₂ leads to variations in the INS spectra level, modifications of the peaks and appearance

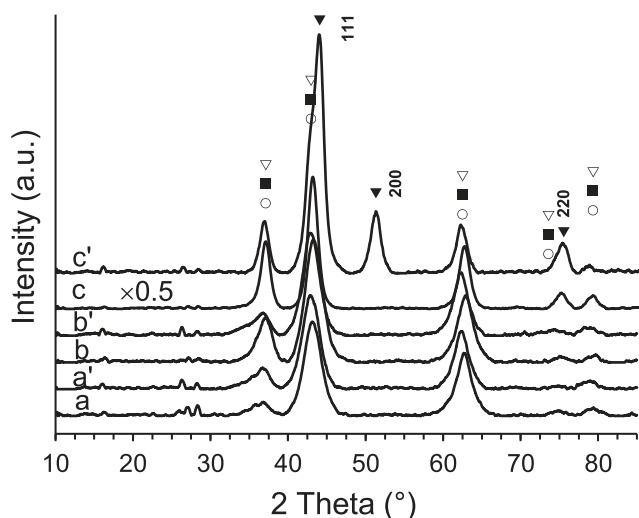


Fig. 7 – XRD patterns obtained after calcination at 500 °C in air (a, b, c) and during in situ treatment in H₂ of Mg₂AlNi_xO_y nano-composites at 450 °C for 10 h (a', b', c'). x = (a, a') 1, (b, b') 3, and (c, c') 12. Ni (▼), NiO (▽), MgO (○) and Mg–(Al)–Ni–O (■).

of new peaks associated with vibration bands of hydrogen (Fig. 8A). New intensive bands are observed after H₂ treatment at 450 °C due to the insertion of different hydrogen species. Some hydrogen species are already present in the Mg₂AlNi_xO_y nano-oxide (before H₂ pre-treatment), even if the solids have been pre-treated under vacuum at 200 °C to eliminate the physisorbed water (Fig. 8B). The vibration bands obtained at about 241, 403 and 621 cm⁻¹ are assigned to hydroxyl groups [28], and are in agreement with the XPS results. To extract more rigorously the new hydrogen species created by the H₂ treatment (Fig. 8C), the INS spectrum of the corresponding oxide treated in vacuum at 200 °C (Fig. 8B) is subtracted to that of Mg₂AlNi_xH₂O_y (treated in H₂ at 450 °C, Fig. 8A). The hydride species associated with the new peaks are clearly visible (at around 645, 927, 1153 and 1774 cm⁻¹ for Mg₂AlNi₃O_y and 613, 790 and 1678 cm⁻¹ for Mg₂AlNi₁₂O_y), even if the spectra are certainly complex contribution from the ternary Mg–Al–Ni–H–O system. As a matter of fact, it was found that magnesium hydride presents two peaks in the range between

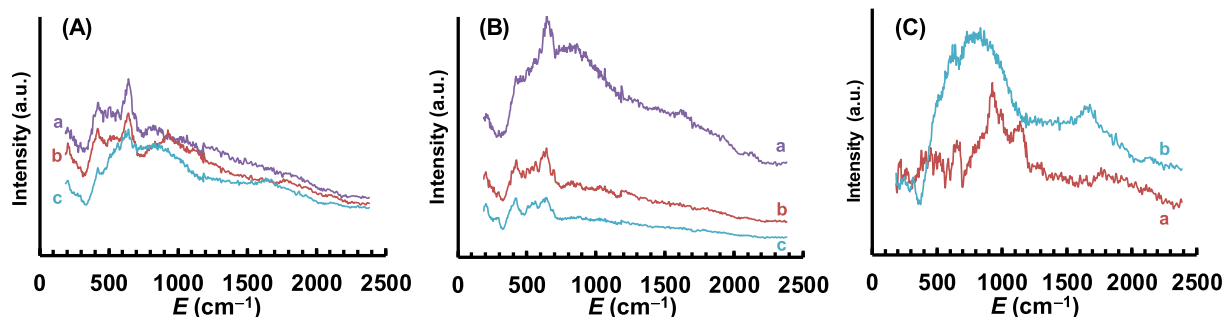
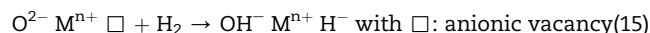


Fig. 8 – INS spectra of Mg₂AlNi_xO_y nano-compounds (A) treated in H₂ at 450 °C for 10 h and (B) treated in vacuum at 200 °C for 2 h. x = (a) 1, (b) 3 and (c) 12. (C) INS spectra of Mg₂AlNi_xH₂O_y after subtraction of Mg₂AlNi_xO_y spectra, x = (a) 3 and (b) 12.

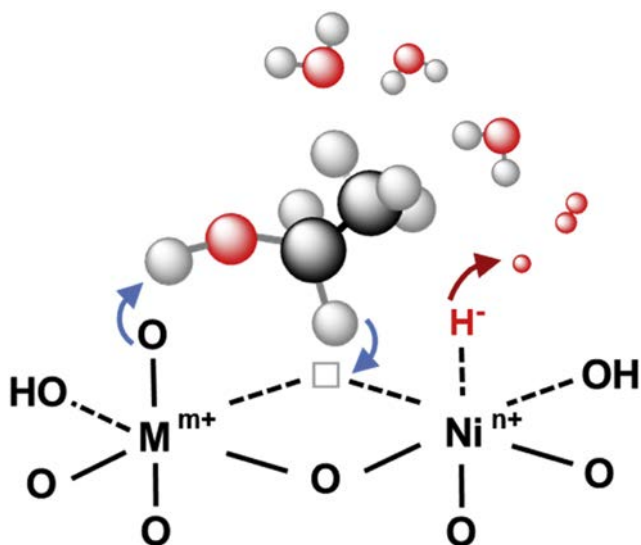
484 and 645 cm⁻¹ [63], aluminum hydride presents a large spectrum with several peaks between 612 and 943 cm⁻¹ [64], and nickel hydride shows broad bands at around 806 and 1613 cm⁻¹ [65]. On the contrary, the Mg₂AlNi₁O_y oxide exhibits a lower spectrum level after H₂ treatment at 450 °C, evidencing no insertion of new hydrogen species under the given conditions. Instead, there is a loss of hydroxyl groups, explained by the higher temperature applied.

Therefore, after treatment in H₂ at 450 °C, all the compounds contain hydroxyl groups and Mg₂AlNi₁O_y compound does not contain hydride species, Mg₂AlNi₃H₂O_y contains hydride species without the presence of metallic Ni⁰, and Mg₂AlNi₁₂H₂O_y contains hydride species with the presence of metallic Ni⁰. After H₂ treatment the solids contain anionic vacancies generated by elimination of H₂O (Eq. (14)) able to capture/receive hydrogen in the form of hydride. Hydrogen can be heterolytically dissociated on an anionic vacancy and an O²⁻ species of the solid (Eq. (15)).



Proposition of active site modeling

Dehydrogenation of ethanol requires the abstraction of hydrogen species from ethanol, with the rupture of C–H bond being the rate-determining step [9–15]. The characterizations of the solids show that the nickel cations are in strong interactions with magnesium and aluminum cations. Therefore, an active site involving cations in strong interaction, an anionic vacancy and an O²⁻ species of the solid can be envisaged for the heterolytic dissociation of ethanol (Eqs. (16) and (17)) leading to the formation of acetaldehyde; H₂ being formed also on the oxyhydride (Eq. (17)). Such a site is modeled in Scheme 1. In presence of high O₂/EtOH ratio (1.6), the easy acetaldehyde transformation in the presence of water and oxygen (Eq. (11)) can explain the results obtained. Moreover, the high reactivity of hydride species with O₂ (exothermicity) generates hydroxyl groups (Eq. (18)), that can further be used for transformation of ethanol to CO₂ and H₂ as it has been shown that abundant OH⁻ groups favor CO transformation to CO₂ by water gas shift (Eq. (10)) [30]. Besides, water can be also dissociated on an anionic vacancy



Scheme 1 – Ethanol activation on $Mg_2AlNi_xH_2O_y$ oxyhydrides. Ni^{n+} : Ni^{2+} or Ni^{8+} , M^{m+} : Mg^{2+} or Al^{3+} and \square : anionic vacancy. The positions of anionic vacancy and hydride species are arbitrary.

and an O^{2-} species of the solid (Eq. (19)). As a matter of fact, it has been shown that water dissociation can be realized when Ni^{2+} species can be stabilized in strong interaction [66]. The high reactivity of hydride species permits consumption of O_2 and then finally transformation of O_2 into the selective O^{2-} species which regenerate the active sites (Eq. (18) followed by Eq. (14)).



Conclusion

Hydrogen production from ethanol has been studied in steam reforming (SRE) and oxidative steam reforming (OSRE) reactions at low temperature over the $Mg_2AlNi_xH_2O_y$ nano-oxyhydride catalysts by applying accurate activation of the catalyst in H_2 and by varying reactants concentration. The insertion of hydride species inside the solid is clearly shown by INS technique with the formation during the treatment in H_2 at 450 °C of $Mg_2AlNi_xH_2O_y$ oxyhydride compounds. The developed catalysts are highly performant whatever in SRE and OSRE conditions, and in particular at very low temperature (≤ 300 °C) with highly stable total conversion of ethanol. Adding O_2 to the feed (OSRE) allows total conversions in harsh conditions and stable H_2 formation for at least 75 h with very low input of energy (50 °C) and decreases carbon formation. Furthermore, a higher production of H_2 can be achieved at 300 °C in OSRE conditions

(60 L h⁻¹ g_{cat}⁻¹) compared to SRE (10 L h⁻¹ g_{cat}⁻¹) when using high concentration of ethanol (14 mol%).

Acknowledgments

This work was financially supported by the Centre National de la Recherche Scientifique France, the National Special Funds of China (C6176102, W. Fang's funding), ECL Lille and Région Hauts de France (Y. Romani's grant), China Scholarship Council (Y. Wei's grant) and Institut Laue Langevin (ILL) Grenoble France. The authors thank Ms. L. Burylo (XRD), Mr. O. Gardoll (TPR, TPO), Ms. M. Trentesaux (XPS) and Mr. J. C. Morin (Raman) from UCCS and Mr. A. Addad (TEM) from "Centre Commun de Microscopie" (CCM) of University of Lille, "plateau technique de la Fédération Chevreul CNRS FR 2638", for their valuable technical assistance. Chevreul Institute (FR 2638), Ministère de l'enseignement Supérieur et de la Recherche, Région Hauts de France, and FEDER are acknowledged for supporting and funding partially this work.

REFERENCES

- [1] Haryanto A, Fernando S, Murali N, Adhikari S. Current status of hydrogen production techniques by steam reforming of ethanol: a review. *Energy Fuels* 2005;19:2098–106.
- [2] Midilli A, Ay M, Dincer I, Rosen MA. On hydrogen and hydrogen energy strategies I: current status and needs. *Renew Sustain Energy Rev* 2005;9:255–71.
- [3] Diethelm S, Van herle J. Ethanol internal steam reforming in intermediate temperature solid oxide fuel cell. *J Power Sources* 2011;196:7355–62.
- [4] Tippawan P, Arpornwichanop A. Performance and economic assessments of a solid oxide fuel cell system with a two-step ethanol-steam-reforming process using CaO sorbent. *J Power Sources* 2016;306:124–34.
- [5] Dou B, Zhang H, Cui G, Wang Z, Jiang B, Wang K, et al. Hydrogen production and reduction of Ni-based oxygen carriers during chemical looping steam reforming of ethanol in a fixed-bed reactor. *Int J Hydrogen Energy* 2017;42:26217–30.
- [6] Dou B, Zhang H, Cui G, Wang Z, Jiang B, Wang K, et al. Hydrogen production by sorption-enhanced chemical looping steam reforming of ethanol in an alternating fixed-bed reactor: sorbent to catalyst ratio dependencies. *Energy Convers Manag* 2018;155:243–52.
- [7] Navarro RM, Peña MA, Fierro JLG. Hydrogen production reactions from carbon Feedstocks: fossil fuels and biomass. *Chem Rev* 2007;107:3952–91.
- [8] Ni M, Leung DYC, Leung MKH. A review on reforming bio-ethanol for hydrogen production. *Int J Hydrogen Energy* 2007;32:3238–47.
- [9] Subramani V, Song C. Advances in catalysis and processes for hydrogen production from ethanol reforming. *Catalysis* 2007;20:65–106. The Royal Society of Chemistry.
- [10] Piscina PRdl, Homs N. Use of biofuels to produce hydrogen (reformation processes). *Chem Soc Rev* 2008;37:2459–67.

- [11] Mattos LV, Jacobs G, Davis BH, Noronha FB. Production of hydrogen from ethanol: review of reaction mechanism and catalyst deactivation. *Chem Rev* 2012;112:4094–123.
- [12] Bion N, Duprez D, Epron F. Design of nanocatalysts for green hydrogen production from bioethanol. *ChemSusChem* 2012;5:76–84.
- [13] Li S, Gong J. Strategies for improving the performance and stability of Ni-based catalysts for reforming reactions. *Chem Soc Rev* 2014;43:7245–56.
- [14] Contreras JL, Salmones J, Colín-Luna JA, Nuño L, Quintana B, Córdova I, et al. Catalysts for H₂ production using the ethanol steam reforming (a review). *Int J Hydrogen Energy* 2014;39:18835–53.
- [15] Li D, Li X, Gong J. Catalytic reforming of oxygenates: state of the art and future prospects. *Chem Rev* 2016;116:11529–653.
- [16] Velu S, Suzuki K, Vijayaraj M, Barman S, Gopinath CS. In situ XPS investigations of Cu_{1-x}Ni_xZnAl-mixed metal oxide catalysts used in the oxidative steam reforming of bio-ethanol. *Appl Catal B* 2005;55:287–99.
- [17] Cai W, Wang F, Zhan E, Van Veen AC, Mirodatos C, Shen W. Hydrogen production from ethanol over Ir/CeO₂ catalysts: a comparative study of steam reforming, partial oxidation and oxidative steam reforming. *J Catal* 2008;257:96–107.
- [18] Biswas P, Kunzru D. Oxidative steam reforming of ethanol over Ni/CeO₂-ZrO₂ catalyst. *Chem Eng J* 2008;136:41–9.
- [19] de Lima SM, da Silva AM, da Costa LOO, Graham UM, Jacobs G, Davis BH, et al. Study of catalyst deactivation and reaction mechanism of steam reforming, partial oxidation, and oxidative steam reforming of ethanol over Co/CeO₂ catalyst. *J Catal* 2009;268:268–81.
- [20] Chiou JYZ, Wang CH, Yang SY, Bi JL, Shen CC, Wang CB. Reforming of ethanol to produce hydrogen over PtRuMg/ZrO₂ catalyst. *J Nanotechnol* 2012;2012:6. <https://doi.org/10.1155/2012/573287>. Article ID 573287.
- [21] Wang Z, Wang H, Liu Y. La_{1-x}Ca_xFe_{1-x}Co_xO₃-a stable catalyst for oxidative steam reforming of ethanol to produce hydrogen. *RSC Adv* 2013;3:10027–36.
- [22] Mondal T, Pant KK, Dalai AK. Oxidative and non-oxidative steam reforming of crude bio-ethanol for hydrogen production over Rh promoted Ni/CeO₂-ZrO₂ catalyst. *Appl Catal A* 2015;499:19–31.
- [23] Mondal T, Pant KK, Dalai AK. Catalytic oxidative steam reforming of bio-ethanol for hydrogen production over Rh promoted Ni/CeO₂-ZrO₂ catalyst. *Int J Hydrogen Energy* 2015;40:2529–44.
- [24] Palma V, Ruocco C, Meloni E, Ricca A. Activity and stability of novel silica – based catalysts for hydrogen production via oxidative steam reforming of ethanol. *Chem Eng Trans* 2016;52:67–72.
- [25] Palma V, Ruocco C, Meloni E, Gallucci F, Ricca A. Enhancing Pt-Ni/CeO₂ performances for ethanol reforming by catalyst supporting on high surface silica. *Catal Today* 2018;307:175–88.
- [26] Greluk M, Rotko M, Machocki A. Conversion of ethanol over Co/CeO₂ and KCo/CeO₂ catalysts for hydrogen production. *Catal Lett* 2016;146:163–73.
- [27] Pirez C, Fang W, Capron M, Paul S, Jobic H, Dumeignil F, et al. Steam reforming, partial oxidation and oxidative steam reforming for hydrogen production from ethanol over cerium nickel based oxyhydride catalyst. *Appl Catal A* 2016;518:78–86.
- [28] Pirez C, Capron M, Jobic H, Dumeignil F, Jalowiecki-Duhamel L. Highly efficient and stable CeNiH₂O_y nano-oxyhydride catalyst for H₂ production from ethanol at room temperature. *Angew Chem Int Ed* 2011;50:10193–7.
- [29] Fang W, Pirez C, Paul S, Capron M, Jobic H, Dumeignil F, et al. Room temperature hydrogen production from ethanol over CeNi_xH₂O_y nano-oxyhydride catalysts. *ChemCatChem* 2013;5:2207–16.
- [30] Liu Z, Senanayake SD, Rodriguez JA. Elucidating the interaction between Ni and CeO_x in ethanol steam reforming catalysts: a perspective of recent studies over model and powder systems. *Appl Catal B* 2016;197:184–97.
- [31] Wu G, Zhang C, Li S, Huang Z, Yan S, Wang S, et al. Sorption enhanced steam reforming of ethanol on Ni–CaO–Al₂O₃ multifunctional catalysts derived from hydrotalcite-like compounds. *Energy Environ Sci* 2012;5:8942–9.
- [32] Zhang C, Zhu W, Li S, Wu G, Ma X, Wang X, et al. Sintering-resistant Ni-based reforming catalysts obtained via the nanoconfinement effect. *Chem Commun* 2013;49(82):9383–5.
- [33] Li S, Zhang C, Huang Z, Wu G, Gong J. A Ni@ZrO₂ nanocomposite for ethanol steam reforming: enhanced stability via strong metal-oxide interaction. *Chem Commun* 2013;49:4226–8.
- [34] Li D, Zeng L, Li X, Wang X, Ma H, Assabumrungrat S, et al. Ceria-promoted Ni/SBA-15 catalysts for ethanol steam reforming with enhanced activity and resistance to deactivation. *Appl Catal B* 2015;176–177:532–41.
- [35] Tian H, Li X, Zeng L, Gong J. Recent advances on the design of group VIII base-metal catalysts with encapsulated structures. *ACS Catal* 2015;5:4959–77.
- [36] Wang T, Ma H, Zeng L, Li D, Tian H, Xiao S, et al. Highly loaded Ni-based catalysts for low temperature ethanol steam reforming. *Nanoscale* 2016;8:10177–87.
- [37] Ma H, Zeng L, Tian H, Li D, Wang X, Li X, et al. Efficient hydrogen production from ethanol steam reforming over La-modified ordered mesoporous Ni-based catalysts. *Appl Catal B* 2016;181:321–31.
- [38] Resini C, Montanari T, Barattini L, Ramis G, Busca G, Presto S, et al. Hydrogen production by ethanol steam reforming over Ni catalysts derived from hydrotalcite-like precursors: catalyst characterization, catalytic activity and reaction path. *Appl Catal A* 2009;355:83–93.
- [39] Coleman LJI, Epling W, Hudgins RR, Croiset E. Ni/Mg–Al mixed oxide catalyst for the steam reforming of ethanol. *Appl Catal A* 2009;363:52–63.
- [40] Li M, Wang X, Li S, Wang S, Ma X. Hydrogen production from ethanol steam reforming over nickel based catalyst derived from Ni/Mg/Al hydrotalcite-like compounds. *Int J Hydrogen Energy* 2010;35:6699–708.
- [41] Lucrédio AF, Bellido JDA, Assaf EM. Effects of adding La and Ce to hydrotalcite-type Ni/Mg/Al catalyst precursors on ethanol steam reforming reactions. *Appl Catal A* 2010;388:77–85.
- [42] Vizcaíno AJ, Lindo M, Carrero A, Calles JA. Hydrogen production by steam reforming of ethanol using Ni catalysts based on ternary mixed oxides prepared by coprecipitation. *Int J Hydrogen Energy* 2012;37:1985–92.
- [43] Fang W, Paul S, Capron M, Dumeignil F, Jalowiecki-Duhamel L. Hydrogen production from bioethanol catalyzed by Ni_xMg₂AlO_y ex-hydrotalcite catalysts. *Appl Catal B* 2014;152–153:370–82.
- [44] Fang W, Paul S, Capron M, Biradar AV, Umbarkar SB, Dongare MK, et al. Highly loaded well dispersed stable Ni species in Ni_xMg₂AlO_y nanocomposites: application to hydrogen production from bioethanol. *Appl Catal B* 2015;166–167:485–96.
- [45] Fang W, Pirez C, Paul S, Jiménez-Ruiz M, Jobic H, Dumeignil F, et al. Advanced functionalized Mg₂AlNi_xH₂O_y nano-oxyhydrides ex-hydrotalcites for hydrogen production from oxidative steam reforming of ethanol. *Int J Hydrogen Energy* 2016;41:15443–52.
- [46] Díaz Alvarado F, Gracia F. Steam reforming of ethanol for hydrogen production: thermodynamic analysis including

- different carbon deposits representation. *Chem Eng J* 2010;165:649–57.
- [47] Akande AJ, Idem RO, Dalai AK. Synthesis, characterization and performance evaluation of Ni/Al₂O₃ catalysts for reforming of crude ethanol for hydrogen production. *Appl Catal A* 2005;287:159–75.
- [48] Yu X-P, Chu W, Wang N, Ma F. Hydrogen production by ethanol steam reforming on NiCuMgAl catalysts derived from hydrotalcite-like precursors. *Catal Lett* 2011;141:1228–36.
- [49] Lorenzuti B, Montini T, De Rogatis L, Canton P, Benedetti A, Fornasiero P. Hydrogen production through alcohol steam reforming on Cu/ZnO-based catalysts. *Appl Catal B* 2011;101:397–408.
- [50] Espinal R, Taboada E, Molins E, Chimentao RJ, Medina F, Llorca J. Cobalt hydrotalcites as catalysts for bioethanol steam reforming. The promoting effect of potassium on catalyst activity and long-term stability. *Appl Catal B* 2012;127:59–67.
- [51] Huang L, Choong C, Chen L, Wang Z, Zhong Z, Campos-Cuerva C, et al. Monometallic carbonyl-derived CeO₂-supported Rh and Co bicomponent catalysts for co-free, high-yield H₂ generation from low-temperature ethanol steam reforming. *ChemCatChem* 2013;5:220–34.
- [52] Chen L, Choong CKS, Zhong Z, Huang L, Ang TP, Hong L, et al. Carbon monoxide-free hydrogen production via low-temperature steam reforming of ethanol over iron-promoted Rh catalyst. *J Catal* 2010;276:197–200.
- [53] Araque M, Vargas JC, Zimmermann Y, Roger A-C. Study of a CeZrCoRh mixed oxide for hydrogen production by ethanol steam reforming. *Int J Hydrogen Energy* 2011;36:1491–502.
- [54] Sato K, Kawano K, Ito A, Takita Y, Nagaoka K. Hydrogen production from bioethanol: oxidative steam reforming of aqueous ethanol triggered by oxidation of Ni/Ce_{0.5}Zr_{0.5}O_{2-x} at low temperature. *ChemSusChem* 2010;3:1364–6.
- [55] Velu S, Satoh N, Gopinath CS, Suzuki K. Oxidative reforming of bio-ethanol over CuNiZnAl mixed oxide catalysts for hydrogen production. *Catal Lett* 2002;82:145–52.
- [56] Palma V, Ruocco C, Meloni E, Ricca A. Oxidative steam reforming of ethanol on mesoporous silica supported Pt-Ni/CeO₂ catalysts. *Int J Hydrogen Energy* 2017;42:1598–608.
- [57] Guil-López R, Navarro RM, Peña MA, Fierro JLG. Hydrogen production by oxidative ethanol reforming on Co, Ni and Cu ex-hydrotalcite catalysts. *Int J Hydrogen Energy* 2011;36:1512–23.
- [58] de Lima SM, da Silva AM, da Costa LOO, Assaf JM, Mattos LV, Sarkari R, et al. Hydrogen production through oxidative steam reforming of ethanol over Ni-based catalysts derived from La_{1-x}Ce_xNiO₃ perovskite-type oxides. *Appl Catal B* 2012;121–122:1–9.
- [59] Sun S, Yan W, Sun P, Chen J. Thermodynamic analysis of ethanol reforming for hydrogen production. *Energy* 2012;44:911–24.
- [60] Armor JN. Overcoming equilibrium limitations in chemical processes. *Appl Catal A* 2001;222:91–9.
- [61] Ponchel A, Huysser A, Lamonier C, Jalowiecki-Duhamel L. CeNi_xO_y and CeAl₂Ni_xO_y solids studied by electron microscopy, XRD, XPS and depth sputtering techniques. *Phys Chem Chem Phys* 2000;2:303–12.
- [62] Lamonier C, Ponchel A, D'Huysser A, Jalowiecki-Duhamel L. Studies of the cerium-metal–oxygen–hydrogen system (metal=Cu, Ni). *Catal Today* 1999;50:247–59.
- [63] Kolesnikov AI, Antonov VE, Efimchenko VS, Granroth G, Klyamkin SN, Levchenko AV, et al. Neutron spectroscopy of magnesium dihydride. *J Alloy Comp* 2011;509(Supplement 2):S599–603.
- [64] Kolesnikov AI, Antonov VE, Markushkin YE, Natkaniec I, Sakharov MK. Lattice dynamics of and by inelastic neutron scattering: high-energy band of optical bond-stretching vibrations. *Phys Rev B* 2007;76:064302.
- [65] Antonov VE, Fedotov VK, Gnesin BA, Grosse G, Ivanov AS, Kolesnikov AI, et al. Anisotropy in the inelastic neutron scattering from fcc NiH. *Europhys Lett* 2000;51:140–6.
- [66] Carrasco J, López-Durán D, Liu Z, Duchoñ T, Evans J, Senanayake SD, et al. Situ and theoretical studies for the dissociation of water on an active Ni/CeO₂ catalyst: importance of strong metal–support interactions for the cleavage of O–H bonds. *Angew Chem Int Ed* 2015;54:3917–21.